Supplementary Information

Opening twisted polymer chains for simultaneously high printability and battery fast-charge

Supporting Figures

Figure S1. Detailed ink preparation process with optical images of each mixing step for the (A) M1, (B) M2, and (C) M3 inks.

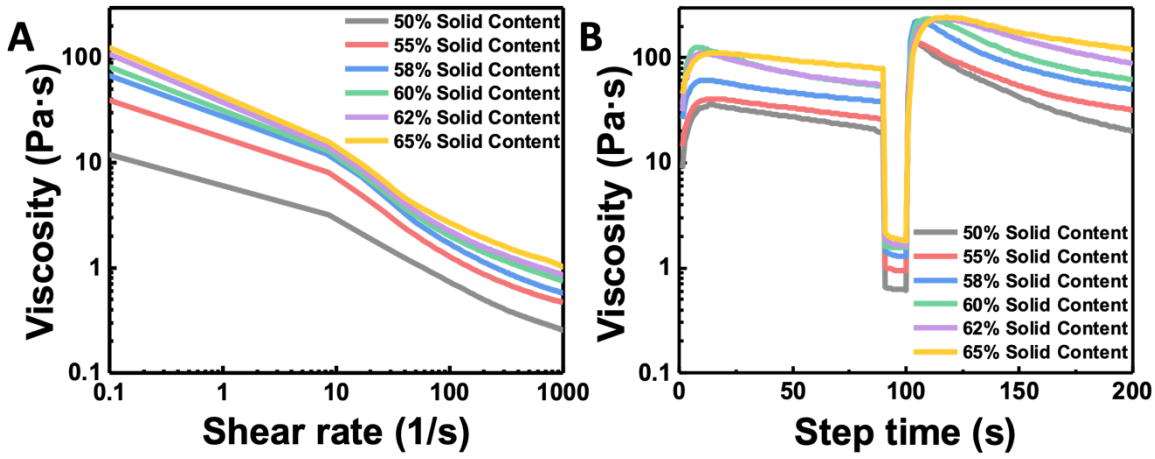

Figure S2. Rheological properties of M1 inks with solid contents from 50% to 65%: (A) viscosity as a function of shear rate and (B) three-step thixotropy test.

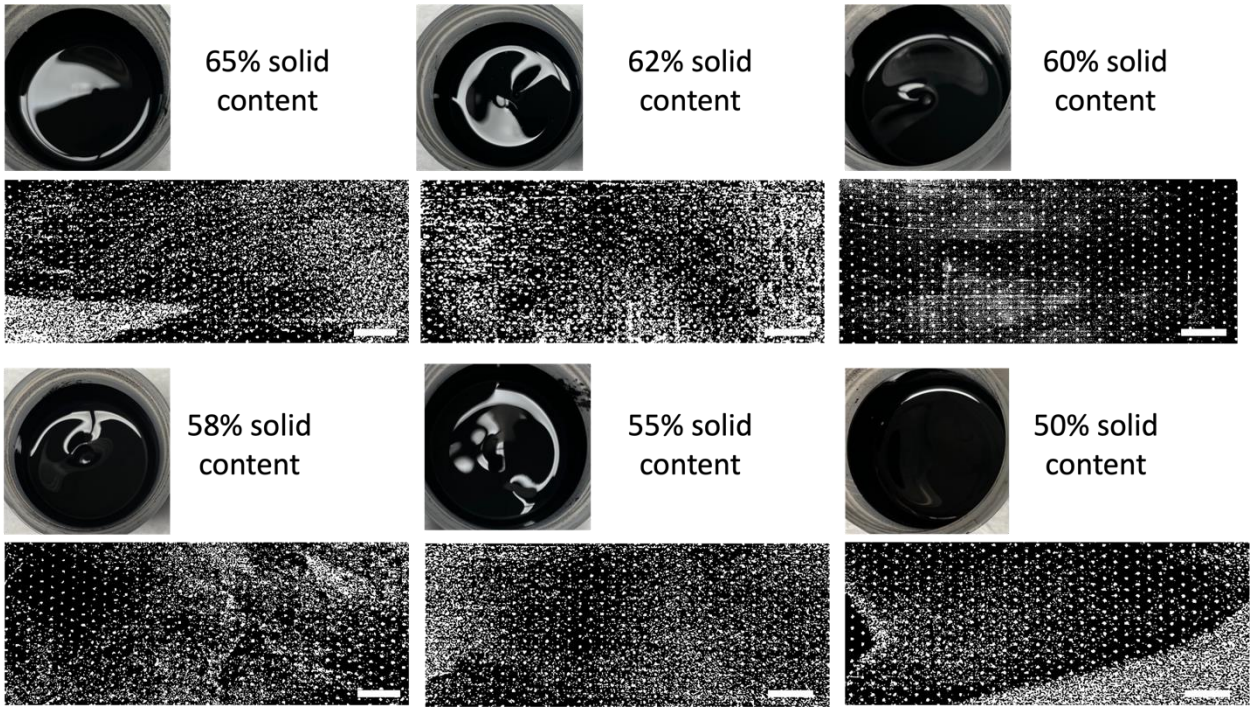

Figure S3. Digital images and printability of M1 inks with solid contents from 65% to 50%. The scale bars are 5 mm in length.

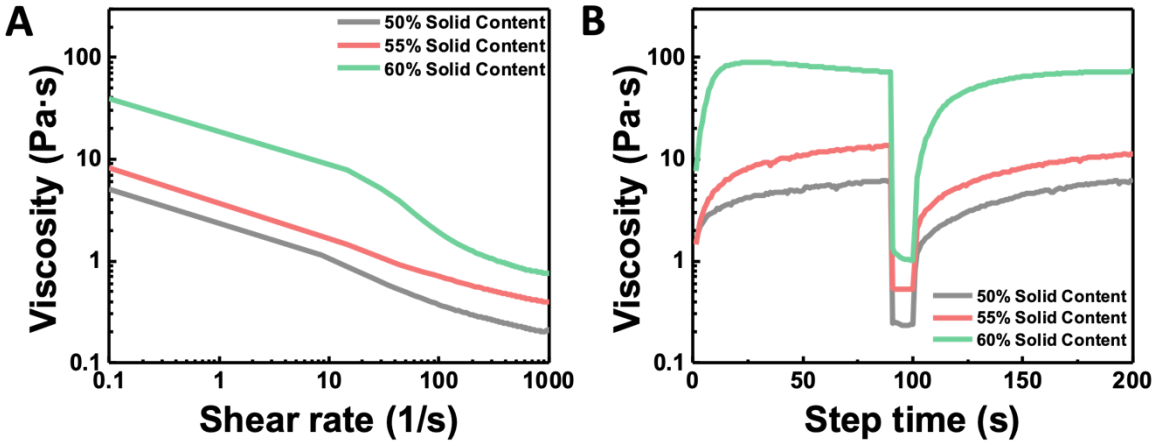

Figure S4. Rheological properties of M2 inks with solid contents from 50% to 60%: (A) viscosity as a function of shear rate and (B) three-step thixotropy test.

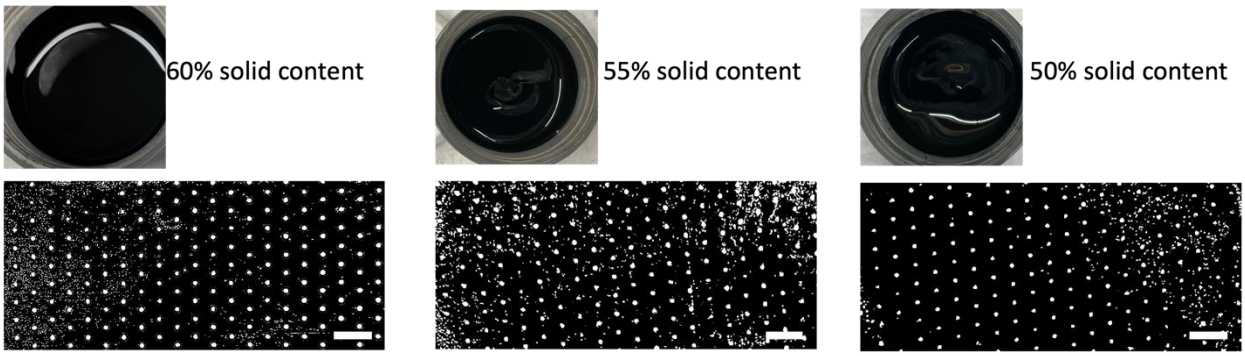

Figure S5. Digital images and printability of M2 inks with solid contents from 60% to 50%. The scale bars are 5 mm in length.

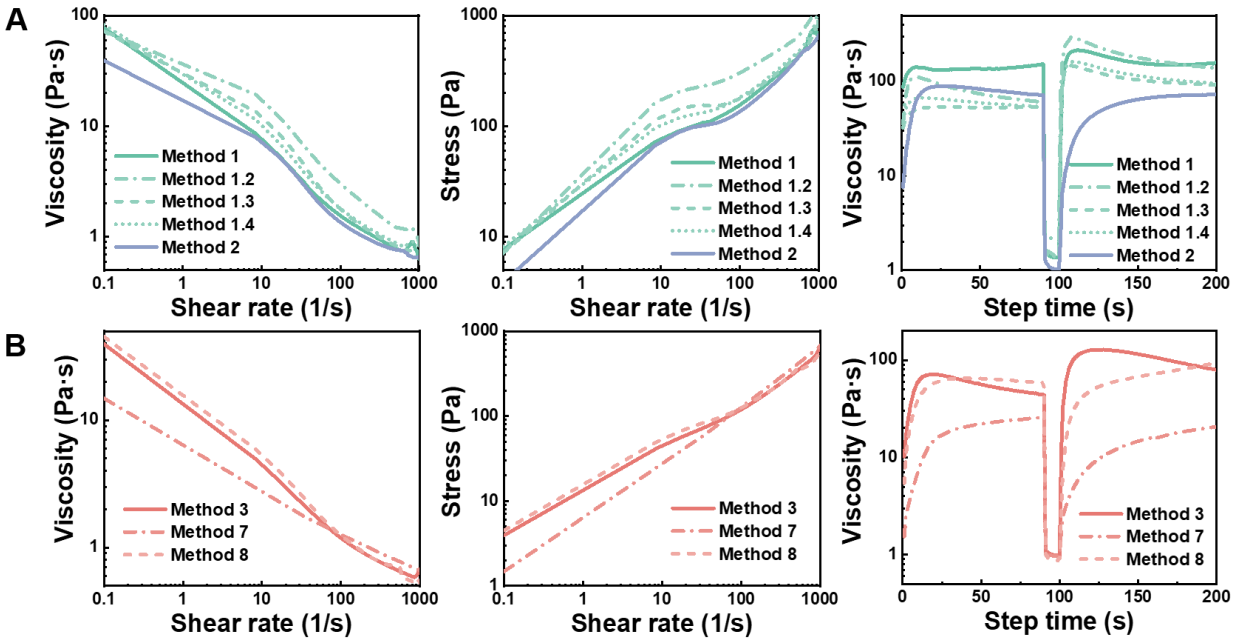

Figure S6. Rheological properties of (A) T-inks and (B) U-inks. The solid content of these inks is 60%. Panel 1: viscosity as a function of shear rate; panel 2: stress as a function of shear rate; and panel 3: three-step thixotropy test (0.1, 200, and 0.1 s^{-1} shear rates were set in three intervals, 0-90 s, 90-100 s, and 100-200 s).

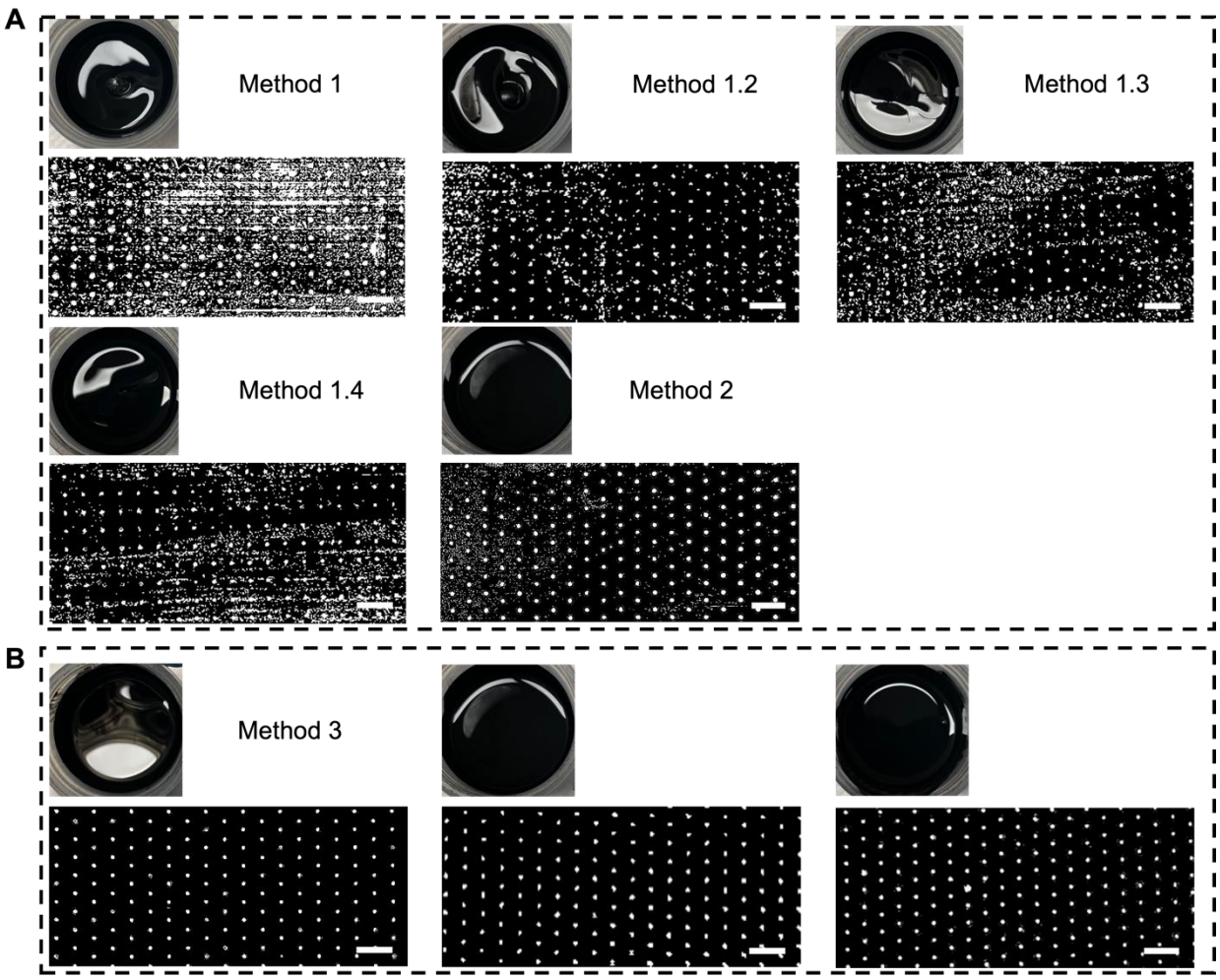

Figure S7. Digital images and printability of (A) T-inks and (B) U-inks. The scale bars are 5 mm in length.

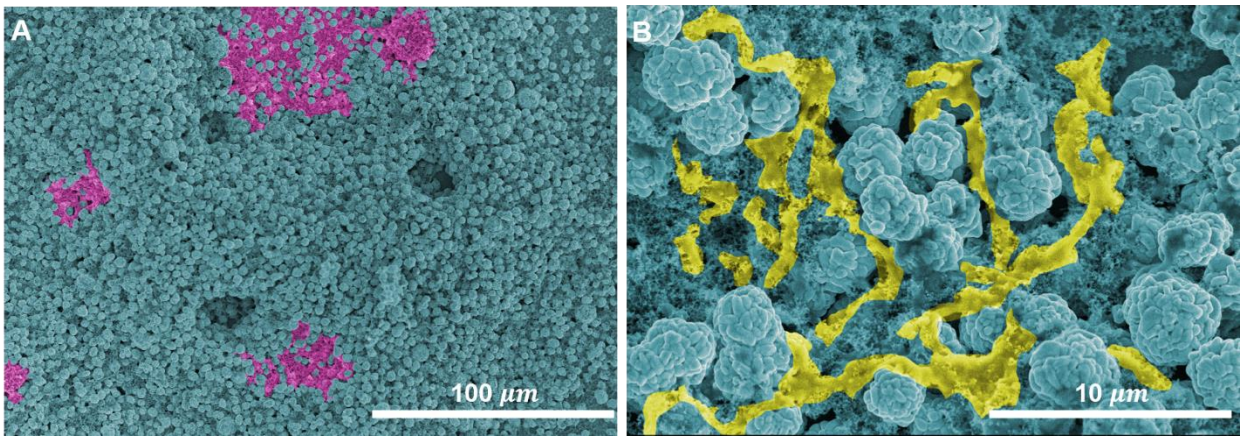

Figure S8. Highlighted images of (A) carbon aggregates (purple) in the M2 electrode and (B) a net-like structure (yellow) in a well-printed region of the M1 electrode, which results from the twisted molecular chains.

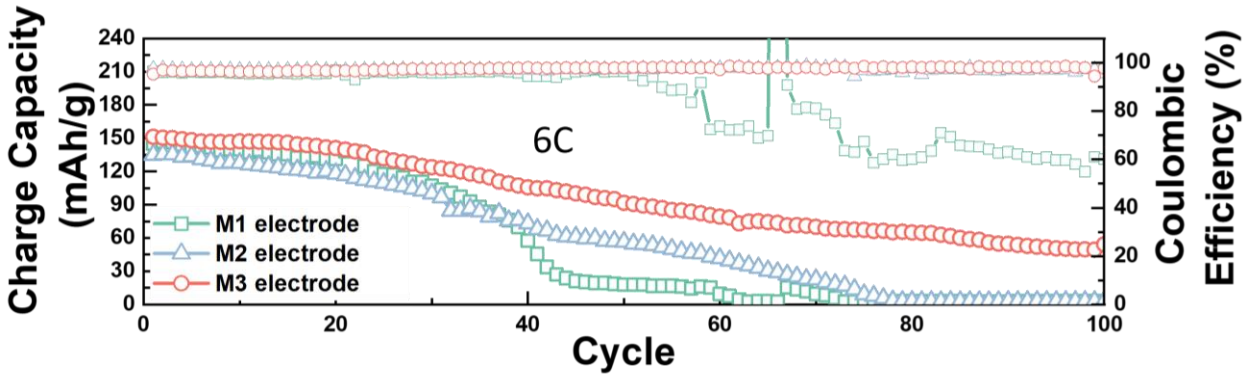

Figure S9. Long-term cycling performance of screen-printed M1, M2, and M3 electrodes at a high rate of 6C. All cells were initially activated at 0.1 C and 0.5 C for three cycles.

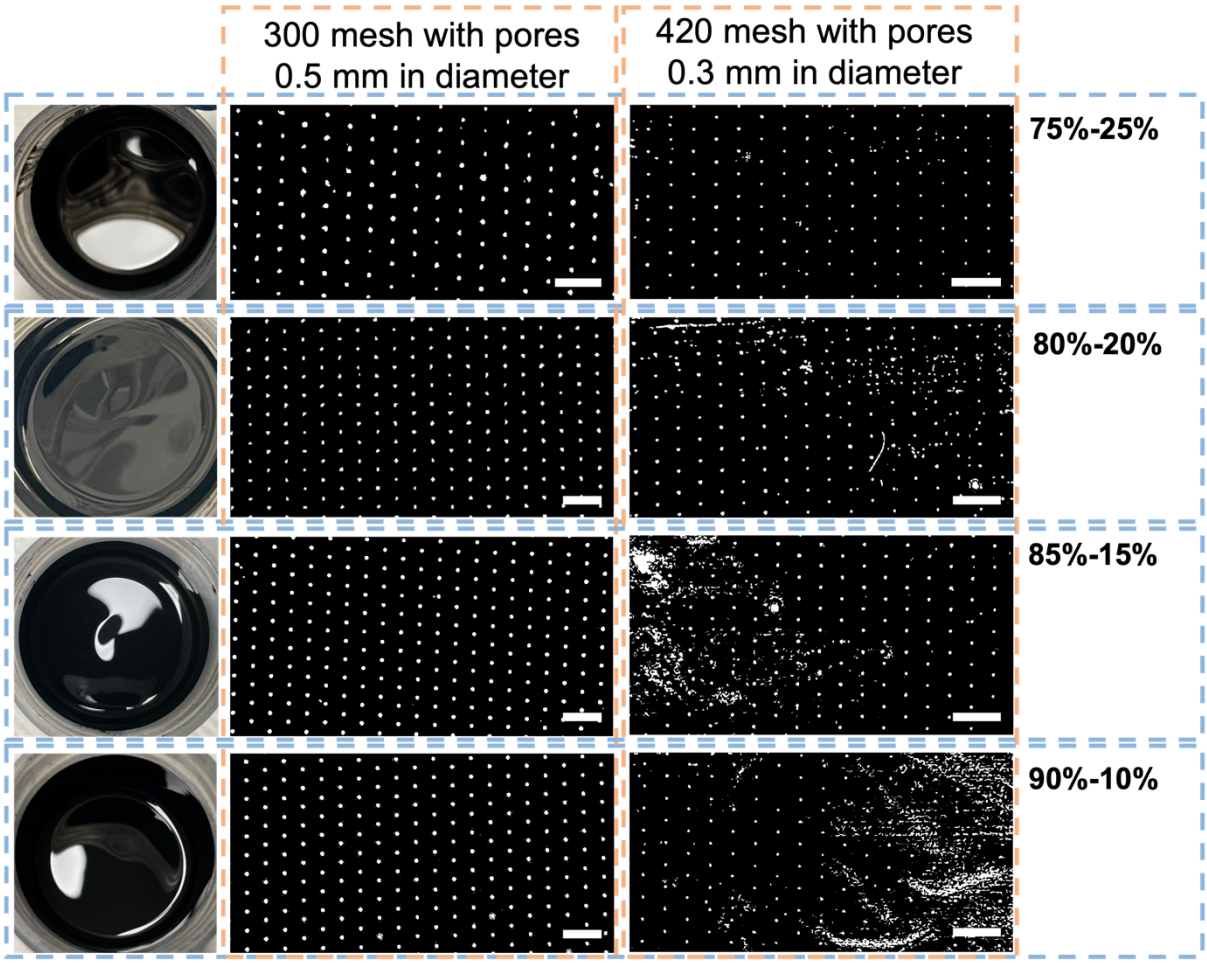

Figure S10. Electrodes screen printed on a bare Al substrate with a 300 mesh screen with pores 0.5 mm in diameter and 420 mesh screen with pores 0.3 mm in diameter. The scale bars are 5 mm in length.

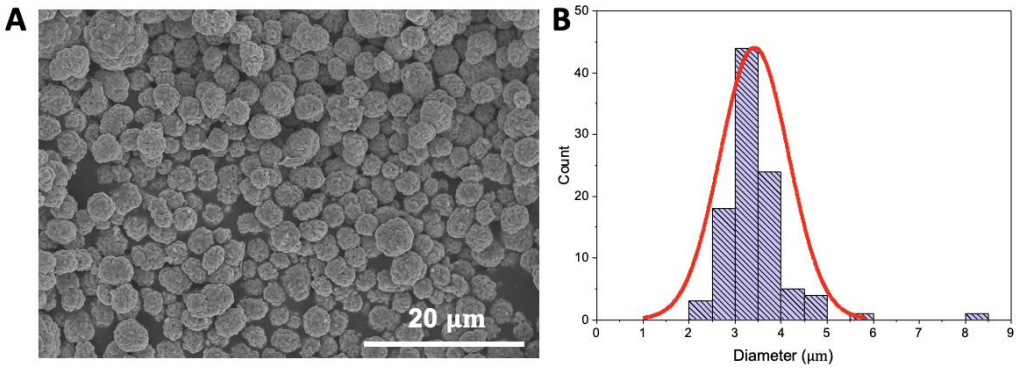

Figure S11. (A) SEM image and (B) size distribution of NMC 622 particles in this work.

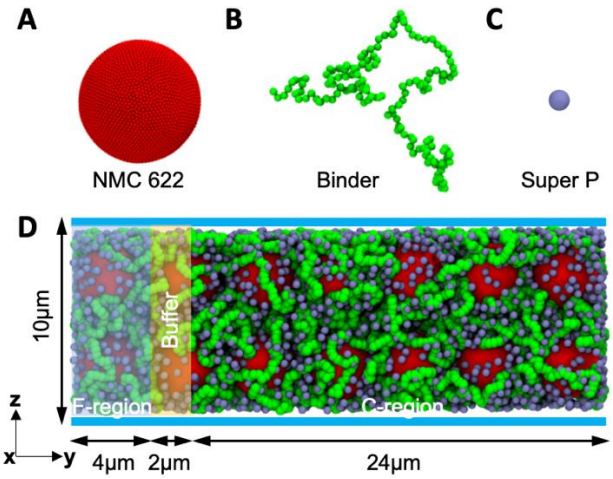

Figure S12. Molecular dynamics models: (A) NMC 622 geometric model. (B) Amorphous binder chain model. (C) Super P particle model. (D) Schematic image of the distribution of different regions in the simulation model. Red denotes NMC 622 particles, green indicates binder chains, and lavender represents Super P particles. The two flat plates along the z-direction are marked in cyan.

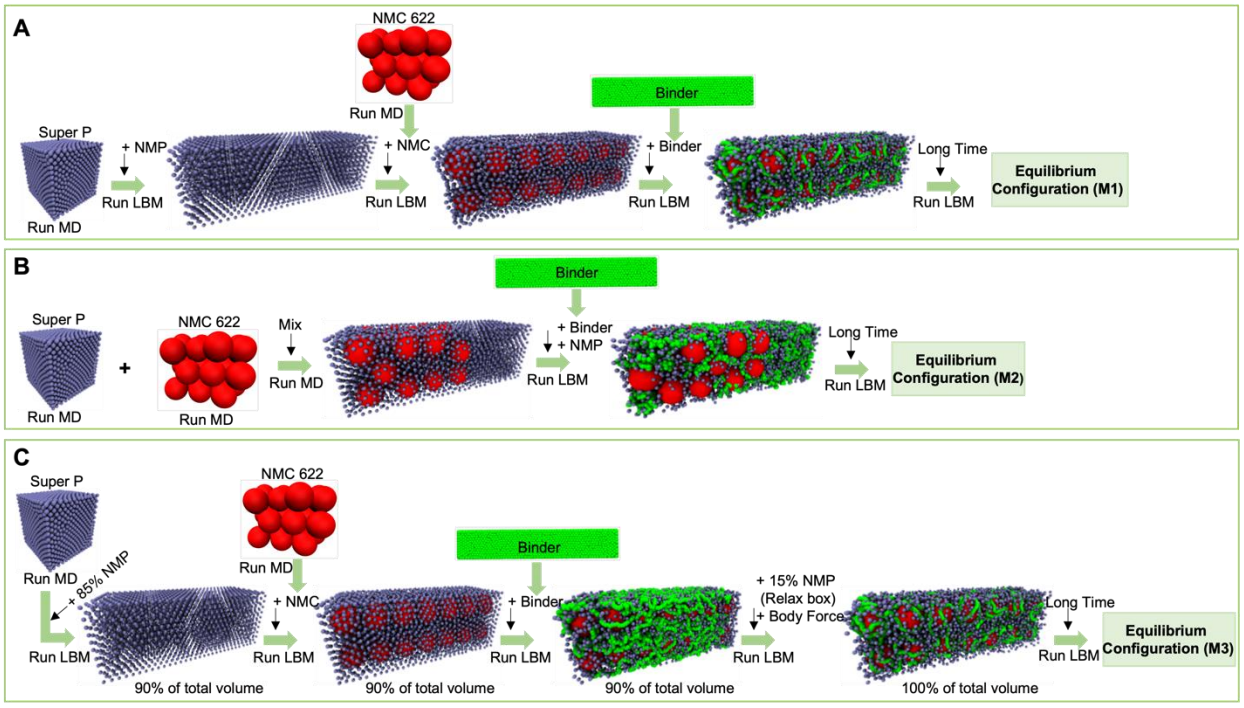

Figure S13. Simulation schematics for the three experimental methods: (A) the M1 method, (B) the M2 method, and (C) the M3 method.

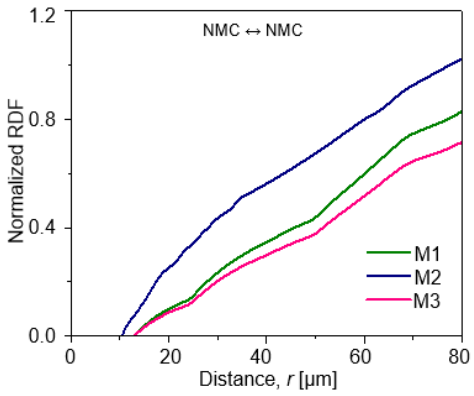

Figure S14. Radial distribution functions (RDFs) of inter-NMC 622 particles for the three methods before shear is applied.

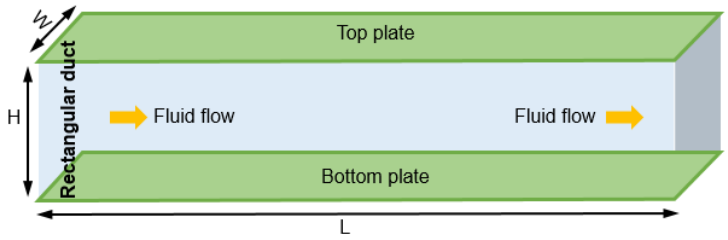

(1). Relationship between shear stress (τ_w) and pressure difference (ΔP);

$$\Delta P \times (WH) = \tau_w \times (2WL)$$

(2). Reconstructing the relationship between τ_w and ΔP;

$$\tau_w = \left(\frac{\Delta P}{2L}\right) \times \left(\frac{WH}{H+W}\right) = \left(\frac{\Delta PH}{2L}\right) \times \left(\frac{1}{H/W+1}\right)$$

(3). Relationship between apparent shear rate ($\dot{\gamma_a}$) and volumetric flow rate (Q);

$$\dot{\gamma_a} = \left(\frac{6Q}{WH^2}\right) \times \left(1 + \frac{H}{W}\right) f^*\left(\frac{H}{W}\right)$$

(4). Relationship between $\log(\tau_w)$ versus $\log(\dot{\gamma_a})$;

(5). Fitting the curve of $\log(\dot{\gamma_a})$ as a function of $\log(\tau_w)$, and obtaining the index *n;*

(6). Obtaining f^*;

$$f^* = \frac{2}{3}(a^* + b^*)$$

(7). Relationship between apparent shear rate ($\dot{\gamma_a}$) and shear rate ($\dot{\gamma_w}$)

$$\dot{\gamma_w} = \dot{\gamma_a}\left(\frac{2}{3}\right)\left(\frac{b^*}{f^*} + \frac{a^*}{f^*}\frac{1}{n}\right)$$

(8). Obtaining the viscosity (μ);

$$\mu = \frac{F}{A}\frac{L}{u} = \frac{\tau_w}{\dot{\gamma_w}}$$

Figure S15. Schematic for obtaining the viscosity of a rectangular duct.

Supporting Tables

Table S1. Details of the ink fabrication processes and a brief summary of the printability and molecular chain conditions for a series of inks.

#	Step 1	Step 2	Step 3	Step 4	Printability	molecular chains situation
1	Mixing the super P and NMP	Add the NMC 622	Add high solid content binder solution	-	**Bad**	Twisted
1.2	Mixing super P and half of binder solution	Add the NMC 622	Add the other half of binder solution	-	**Bad**	Twisted
1.3	Pre-mixing the powders for 1 h at 500 rpm	Add NMP	Add half of high solid content binder solution	Add the other half of high solid content binder solution	**Bad**	Twisted
1.4	Mixing the super P and 1/2 NMP	add the other 1/2 of NMP	Add NMC 622	Add high solid content binder solution	**Bad**	Twisted
2	Mixing powders by hand milling	Add binder solution	-	-	**Bad**	Twisted
3	Mixing Super P and part of NMP	Add NMC 622	Add high solid content binder solution	Add the other part of NMP	**Good**	Untwisted
3.2	Mixing powders by hand milling	Add NMP	Add high solid content binder solution	Add NMP step by step	**Good**	Untwisted
3.3	Pre-mixing the powders for 1 h at 500 rpm	Add part of NMP	Add high solid content binder solution	Add the other part of NMP	**Good**	Untwisted

Table S2. Coarse-grained potential parameters for all particles in the simulation with their corresponding physical values.

Parameters	Simulation (LJ unit)	Physical
Simulation box size ($L_x \times L_y \times L_z$)	40 × 120 × 40	10 × 30 × 10 μm
Super P (mass/volume fraction)	2.4%/2.06%	2.4%/2.06%
NMC622 (mass/volume fraction)	56.40%/33.55%	56.40%/33.55%
Binder (mass/volume fraction)	1.20%/1.10%	1.20%/1.10%
NMP solvent (mass/volume fraction)	40%/63.29%	40%/63.29%
Energy scale (k_BT)	1.0519×10^{-5}	4.1418×10^{-21} N m
NMC622 diameter (D)	14.00	3.500×10^{-6} m
Chain length of binder (l_p)	87.6	2.190×10^{-5} m
Equilibrium bond length of binder (l_0)	0.60	1.500×10^{-7} m
Viscosity of fluid (η)	0.263	1.890×10^{-3} Pa s
Sphere area constant (k_a)	7.4921×10^{-2}	4.72×10^{-5} N m^{-1}
Sphere shear modulus (μ_r)	1.00	6.30×10^{-4} N m^{-1}

Sphere local area constant (k_d)	3.6667	2.31×10^{-3} N m^{-1}
Sphere volume constant (k_v)	0.9881	2.490×10^{3} N m^{-2}
Sphere bending constant (k_b)	0.1270	5.000×10^{-18} N m
Polymer stretching constant (k_{sp})	1.00	6.30×10^{-4} N m^{-1}
Polymer bending constant (k_b)	5.259×10^{-4}	2.0709×10^{-19} N m^{-1}
Morse energy well width (β)	0.96	3.84×10^{6} m^{-1}
Morse energy (D_0)	3.160×10^{-6}	1.2425×10^{-22} N m^{-1}
Morse equilibrium distance (r_0)	2.00	5.000×10^{-7} m
Morse cutoff (r_c)	6.00	1.500×10^{-6} m
LJ depth of well (ϵ)	1.050×10^{-4}	4.14×10^{-21} N m
LJ zero potential distance (σ)	2.00	5.000×10^{-7} m
LJ cutoff distance (r_{lj})	2.24	5.600×10^{-7} m